General Disclaimer

One or more of the Following Statements may affect this Document

- This document has been reproduced from the best copy furnished by the organizational source. It is being released in the interest of making available as much information as possible.

- This document may contain data, which exceeds the sheet parameters. It was furnished in this condition by the organizational source and is the best copy available.

- This document may contain tone-on-tone or color graphs, charts and/or pictures, which have been reproduced in black and white.

- This document is paginated as submitted by the original source.

- Portions of this document are not fully legible due to the historical nature of some of the material. However, it is the best reproduction available from the original submission.

2
CONFERENCES

As explained in the introduction, a good deal of effort was put into preparing, attending, and following up meetings and conferences of various kinds. The information generated by these activities was transferred to MSC verbally at these meetings and by letters at subsequent times. In a few cases, information was generated in response to letters or phone calls from MSC personnel and transmitted to MSC in a similar way.

2.1. TRAVEL

Trips made by Willow Run Laboratories' personnel under this program are listed below.

Date	Willow Run Laboratories' Personnel	Organization Visited	Purpose of Visit
8/16/67	M. Bair	University of Nevada	To attend passive microwave team meeting
9/11/67	D. Lowe and J. Braithwaite	NASA MSC	To review program with sponsor
10/10/67	D. Lowe and M. Holter	NASA MSC	To discuss 1A program development plan for spacecraft experiments
10/19/67	J. Braithwaite and J. Cook	NASA MSC	To discuss 1A experiments
11/7/67	W. Brown and J. Cook	Night Vision Laboratory, Ft. Belvoir, Virginia	To discuss cryogenics state of the art
11/3/67	J. Cook and W. Brown	Block Associates and Honeywell Corporation, Boston	To discuss spectrometer design and cryogenics and detector technology
11/13/67	J. Braithwaite and J. Cook	Optical Coating Laboratories, Santa Rosa, Calif.	To discuss state of the art of interference filters and dichoric mirrors
11/14/67	J. Braithwaite and J. Cook	Lockheed Missiles and Spacecraft Company, Sunnyvale, Calif.	To discuss SW spectrometer design and cryogenics technology
11/15/67	D. Lowe and P. Hasell	Martin-Marietta, Denver: Santa Barbara Research Center & Aerojet General	To discuss Apollo Applications experiments
11/21/67	J. Braithwaite	NASA, Goddard	To discuss Long Wavelength spectrometer experiment design
11/22/67	E. Work	IIT Research Institute	To acquire information on current state of the art of fiber optics
11/27/67	J. Braithwaite	NASA MSC	To attend meeting on ground truth test site instrumentation requirements

NOTICES

Sponsorship. The work reported herein was conducted by the Willow Run Laboratories of the Institute of Science and Technology for the National Aeronautics and Space Administration's Manned Spacecraft Center under Contract NAS9-7156. Contracts and grants to The University of Michigan for the support of sponsored research are administered through the Office of the Vice-President for Research.

FINAL REPORT ON INFRARED SYSTEM STUDIES FOR THE EARTH RESOURCE PROGRAM

J. Braithwaite
J. J. Cook
W. Brown

October 1968

Prepared under Contract NAS9-7156 by
Willow Run Laboratories
Institute of Science and Technology
The University of Michigan
Ann Arbor, Michigan

NATIONAL AERONAUTICS AND SPACE ADMINISTRATION

FOREWORD

The work described in this report was conducted by the Infrared and Optical Sensor Laboratory of Willow Run Laboratories, a unit of The University of Michigan's Institute of Science and Technology. D. Lowe was Principle Investigator. The following people were responsible for specific aspects of the work and the corresponding sections of the report:

J. Cook	Short Wavelength Spectrometer
W. Brown	Ultraviolet Imaging
J. Braithwaite	Path Transmission Effects and Optimum Optical Bandwidths

The work reported is closely related to the comparative multispectral remote sensing program at Willow Run Laboratories in which improvements are sought in the kinds and qualities of data obtainable and in the quality, speed, and economy of the image interpretation process.

This research was performed for NASA's Manned Spacecraft Center under Contract NAS9-7156, and is similar to and in many respects dependent upon the work completed by Willow Run Laboratories for the U. S. Geological Survey under Contracts 14-08-001-10053 and 14-08-001-10108, for NASA's Marshall Space Flight Center under Contract NAS-8-21000, and for the U. S. Department of Agriculture under Contract NsG 715. The Willow Run Laboratories report number is 1059-11-F.

SUMMARY

The work described in this report was closely related to and closely coordinated with the Earth Resource Program which is being conducted by NASA's Manned Spacecraft Center.

The many conferences, meetings, and visits relating to this program in which Willow Run Laboratories' personnel took part are listed and very briefly described. The work carried out in support of NASA plans for the AAP/1A mission are summarized.

The results of a preliminary design study for a short wavelength spectrometer are given in parametric form. A study of the relative merits of scanners and cameras showed that the practical limitations of these systems are so different that a generalized comparison in useful form is virtually impossible. The practicality of obtaining terrain surface temperatures from radiances measured from orbit was analyzed. It is shown that the accuracy achieved depends on how well the humidity of the lower atmosphere is known. As a result, residual errors may be serious for situations involving low latitudes and low terrain altitudes if good humidity data is not available, but these errors are negligible in polar regions for most purposes. A brief account of the current relative merits of the various detector cryogenic systems for orbital use is given. A theorem on the SNR requirements of a multispectral sensor is proved which shows that high SNR is not necessary if a large number of effective channels can be used.

CONTENTS

FIGURES

TABLES

FINAL REPORT ON INFRARED SYSTEM STUDIES FOR THE EARTH RESOURCE PROGRAM

1 INTRODUCTION

The work described in this report was carried out between 22 June 1967 and 21 June 1968 under a contract with NASA's Manned Spacecraft Center (MSC) in Houston, Texas. The research, which was closely coordinated with appropriate personnel at MSC, can be reported most conveniently in three parts as follows:

(1) Conferences and meetings were held on the subject of NASA's Earth Resource Program. Most of these conferences were called by NASA and held at MSC, although some visits to NASA headquarters and other organizations and visits by NASA personnel to Willow Run Laboratories fall in this category. In many cases, time was spent preparing presentations or data for these meetings, and a frequent result of the meetings was effort directed toward analysis and formulation of infrared experiments and hardware for either aircraft or spacecraft use and review and recommendations concerning aircraft sensors. This work is summarized in section 2 of this report.

(2) Investigations and documentation relating directly to the AAP (Apollo Application Program)/1A experiments, S102 (the dual channel scanner) and S103 (the short wavelength spectrometer), were carried out. Effort included analysis and definition of experiments and hardware specifications and discussions with prospective hardware manufacturers and component suppliers. At the time that project was cancelled, statements of work for the procurement of the experimental hardware had been completed. This work is described in section 3 of this report.

(3) Independent studies were carried out on aspects of remote sensing which seemed to require investigation. By and large, these problems arose in connection with one of the tasks described above. Accounts of these studies are given in section 4.

It should be noted that the work carried out and described here represents a merging and continuation of two streams of investigation previously accomplished by Willow Run Laboratories: the application of infrared techniques to remote sensing and the application of infrared techniques used in orbital vehicles to lunar surface and earth resources problems. Research in the latter area was funded by the U. S. Geological Survey and the U. S. Department of Agriculture.

2
CONFERENCES

As explained in the introduction, a good deal of effort was put into preparing, attending, and following up meetings and conferences of various kinds. The information generated by these activities was transferred to MSC verbally at these meetings and by letters at subsequent times. In a few cases, information was generated in response to letters or phone calls from MSC personnel and transmitted to MSC in a similar way.

2.1. TRAVEL

Trips made by Willow Run Laboratories' personnel under this program are listed below.

Date	Willow Run Laboratories' Personnel	Organization Visited	Purpose of Visit
8/16/67	M. Bair	University of Nevada	To attend passive microwave team meeting
9/11/67	D. Lowe and J. Braithwaite	NASA MSC	To review program with sponsor
10/10/67	D. Lowe and M. Holter	NASA MSC	To discuss 1A program development plan for spacecraft experiments
10/19/67	J. Braithwaite and J. Cook	NASA MSC	To discuss 1A experiments
11/7/67	W. Brown and J. Cook	Night Vision Laboratory, Ft. Belvoir, Virginia	To discuss cryogenics state of the art
11/3/67	J. Cook and W. Brown	Block Associates and Honeywell Corporation, Boston	To discuss spectrometer design and cryogenics and detector technology
11/13/67	J. Braithwaite and J. Cook	Optical Coating Laboratories, Santa Rosa, Calif.	To discuss state of the art of interference filters and dichoric mirrors
11/14/67	J. Braithwaite and J. Cook	Lockheed Missiles and Spacecraft Company, Sunnyvale, Calif.	To discuss SW spectrometer design and cryogenics technology
11/15/67	D. Lowe and P. Hasell	Martin-Marietta, Denver: Santa Barbara Research Center & Aerojet General	To discuss Apollo Applications experiments
11/21/67	J. Braithwaite	NASA, Goddard	To discuss Long Wavelength spectrometer experiment design
11/22/67	E. Work	IIT Research Institute	To acquire information on current state of the art of fiber optics
11/27/67	J. Braithwaite	NASA MSC	To attend meeting on ground truth test site instrumentation requirements

Date	Willow Run Laboratories' Personnel	Organization Visited	Purpose of Visit
12/6/67	D. Lowe and P. Hasell	Texas Instruments	To discuss scanner design for 1A
12/19/67	P. Hasell and J. Braithwaite	International Telephone and Telegraph, Fort Wayne, Ind.	To discuss scanner design and passive cooling techniques
1/22/68	D. Lowe	Texas A&M University	To attend ninth meeting of ad hoc spacecraft oceanography advisory group
1/24/68	D. Lowe	NASA MSC	To attend eleventh inflight experimenters meeting
2/9/68	D. Lowe	NASA Headquarters	To discuss infrared instrumentation team activities
2/13/68	D. Lowe	NASA MSC	To discuss various aspects of the program
2/27/68	P. Hasell and L. Larsen	Texas Instruments	To consult with Texas Instruments and NASA on NASA dual-channel scanner procurement
2/22/68	P. Hasell and L. Larsen	NASA MSC	To consult with NASA on airborne scanners
2/27/68	D. Lowe	NASA Headquarters	To participate in meeting on space electro-optical imaging systems
3/4/68	D. Lowe	University of Kansas	To attend radar team meeting
3/19/68	D. Lowe	NASA MSC	To participate in meeting on field measurement requirements for earth resources ground truth
3/24/68	R. Knighton		To attend EEE Linear Integrated Circuit Clinic in New York
4/30/68	M. Holter	NASA MSC	To discuss multispectral sensing program and capabilities
5/28/68	M. Holter	NASA, Electronics Research Center	To discuss earth resource sensing
6/23/68	D. Lowe	Los Angeles	To attend Third AIAA Thermophysics Conference and committee meeting
6/25/68	D. Lowe	NASA MSC	To discuss project
6/6/68	J. Cook	A. D. Little Cambridge, Mass.	To discuss cryogenic system

2.2. VISITORS

The people listed below visited Willow Run Laboratories for the express purpose of discussing some aspect of the program.

Date	Personnel	Affiliation	Purpose
10/27/67	L. Childs	NASA MSC	Program review
10/27/67	W. Green	NASA MSC	Program review
11/29/67	D. LaFace	Marshall Laboratories	To discuss 1A experiments
11/29/67	G. Spellman	Marshall Laboratories	To discuss 1A experiments
12/12/67	W. Burnett	HRB-Singer	To discuss 1A scanner experiments
12/12/67	J. Walker	HRB-Singer	To discuss 1A scanner experiments
1/12/68	N. Foster	NASA MSC	To discuss multispectral sensing
1/12/68	B. Sobels	Bell Communications Laboratories	To discuss multispectral sensing
2/2/68	B. Hand	NASA MSC	To discuss ground truth instrumentation requirements
2/2/68	B. Edwards	NASA MSC	To discuss ground truth instrumentation requirements
2/2/68	O. Smistad	NASA MSC	To discuss ground truth instrumentation requirements
2/26/68	R. Richard	NASA MSC	To discuss multispectral sensing
3/2/68	W. Eichelman	NASA MSC	To work up program development plan for experiments S102 and S103
6/12/68	L. Childs	NASA MSC	Program review

2.3. CONFERENCE ON INFRARED INSTRUMENTATION

In conjunction with the Fifth Remote Sensing Symposium, a meeting was held on 16 April 1968 to discuss infrared instrumentation aspects of the NASA Earth Resource Program. All users of infrared data from the NASA aircraft program and those interested in spaceborne infrared experiments in earth resourse applications were invited to attend. Some of the topics considered are:

Current program objectives
Status of infrared instrumentation in aircraft
Proposed improvements in infrared instrumentation
Requirements for data from high altitude aircraft
RB-57 instrumentation recommendations
Program development plans for space experiments

The attendees and their affiliation were:

W. Allen - USDA, Weslaco
D. Anderson - USGS
D. Carter - USGS
C. Centers - NASA Headquarters
L. Childs - NASA MSC
J. Cook - Willow Run Laboratories
J. Lintz - University of Nevada
D. S. Lowe - Willow Run Laboratories
R. Lyon - Stanford University
R. MacDonald - Purdue
R. Marshall - Willow Run Laboratories
R. Miller - USDA

S. Garawecki - USGS
H. Gausman - USDA, Weslaco
T. George - NASA Headquarters
A. Gerlach - USGS
R. Holmes - Purdue
T. Phillips - Purdue
F. Polcyn - Willow Run Laboratories
D. Simonette - University of Kansas
O. Smistad - NASA MSC
C. Wiegand - USDA, Weslaco

3
THE AAP/1A PROGRAM

A great deal of effort went into investigations and documentation relating directly to the projected AAP/1A experiments S102 (the dual channel scanner) and S103 (the short wavelength spectrometer). The result of this effort was work statements for the two experiments and for requests for proposals. The latter were prepared as part of a plan to procure the instrumentation for the experiments by means of subcontracts. However, the 1A program was cancelled before these requests for proposals were released. As the specifications for this hardware are now primarily of historical interest and are presumably on file at MSC, they are not repeated here.

The effort involved updating instrument specifications which had been generated under earlier exercises and in particular insuring that the specifications were compatible with the constraints imposed by the 1A flight plans and the 1A Experiment Carrier (EC) and its data handling facilities. This included analysis of the various interfaces especially insofar as these affected data rates and bulk and discussions with MSC and Martin (the experiment integration contractor) personnel. In view of the very short development time projected for the program, visits were made to several prospective suppliers of critical components and subsystems and to the leading contenders for the hardware subcontracts. This was done to ensure, insofar as possible, that the program would not be hindered by misunderstanding and misconceptions when contracts and subcontracts were finally let. These visits are listed in section 2.1.

4
INDEPENDENT STUDIES

4.1. SHORT WAVELENGTH SPECTROMETER

Discussions with representatives of various user agencies have indicated the desirability of simultaneous multispectral imagery of the earth's surface. These agencies believe that such imagery would help achieve various goals in their disciplines (agriculture, forestry, geology, oceanography, etc.). A multispectral scanning device offers the most convenient

means of data collection to generate this imagery. The advantage of this device is its output format in which the data appear directly in electronic form, convenient for transmission, storage, and analysis.

However, in order to achieve goals such as detection and identification of vegetation types, agricultural crops, geologic assemblages, and similar terrain features, it is necessary to understand the effects of spectral and spatial resolution and of spectral band coverage. Spectral data which are presently being obtained in laboratory and ground-based field measurements indicate unique spectral patterns and therefore diagnostic potential. However, the effect of the intervening atmosphere on this type of data obtained from airborne and spaceborne platforms is not completely understood (some aspects of this problem are dealt with in more detail in section 4.3). In the absence of a firm understanding of atmospheric effects, not only is it impossible to predict corrections for atmospheric absorption, emission, and scattering, but optimum selection of spectral bands and bandwidths cannot be made. This, together with the narrow and often highly complex spectral bands involved in an identification, indicate the need for spectral resolution experimentation over a wide wavelength range from both airborne and spaceborne platforms. Such data would be used to indicate any degradation in diagnostic potential from that available in ground-based measurements and to establish correction methods for application to remotely sensed spectra.

SNR and data-rate considerations limit spatial and spectral resolution and the number of channels of present, state-of-the-art multispectral imagers. As a result, these devices are poorly suited to the task of assessing the effect of such factors as atmospheric absorption or scattering on remotely sensed spectral signatures. Ultimately, the multispectral imager represents an ideal data collection device for experimental and operational systems. In the meantime, however, it becomes advantageous to conduct experimental measurements with a high spectral resolution spectrometer which would, ideally, be coupled with an imaging device such as a boresighted camera or an optical-mechanical scanner. The imager would generate high spatial-resolution imagery in one (or a few) relatively broad spectral interval(s), while the spectrometer would gather high spectral-resolution data along a single path across the scene (the platform ground track). In fact, even when complex and versatile multispectral imagers are available, such a spectrometer would still have value for the collection of spectra of specific objects at better spectral resolution than would be practicable with the imager.

With these factors in mind, a preliminary analysis has been performed aimed at a better understanding of the parametric relations and trade offs involved in spectrometer design specifications.

4.1.1. PERFORMANCE: THE PARAMETRIC EQUATION. In the design of a short wavelength spectrometer, a variety of trade offs exist among such parameters as spatial and spectral resolution, ground coverage, detector type and size, and the diameter and configuration of the collecting optics. In order to understand better the nature of the relation of these pa-

rameters to overall system performance, consider an expression for the output SNR using a given set of operating characteristics:

$$SNR = \frac{\sigma \beta^2 D^2 \tau \Delta\rho D^*_\lambda H_\lambda \Delta\lambda}{4\sqrt{A\,\Delta f}} \qquad (1)$$

where σ = square wave to rms conversion factor = 0.45

β = system spatial resolution (rad)

D = diameter of collecting optics (cm)

τ = transmission of total path, target scene to detector

$\Delta\rho$ = reflectance difference in target scene

D^*_λ = spectral detectivity of sensitive element ($cm\text{-}Hz^{1/2}W^{-1}$)

A = area of detector (cm^2)

H_λ = solar spectral irradiance ($W\text{-}cm^{-2}\,\mu m^{-1}$)

$\Delta\lambda$ = system spectral resolution (μm)

Δf = system electrical bandwidth (Hz)

Certain of these parameters will be established by state-of-the-art performance capabilities, others by weight and size considerations, and still others by the goals of a given mission. Each will be discussed in the following section according to the nature of their limitations and the various trade-offs to be considered in a final design selection.

4.1.2. PARAMETRIC TRADE OFF CONSIDERATIONS

4.1.2.1. Spatial Resolution. Several institutions are currently investigating the use of spectral information to identify various terrain features or conditions such as soil and crop identification, water pollution, vegetational moisture stress, fish detection, and shoal mapping. Laboratory and ground-based field measurements indicate that spectral patterns offer a potential means of rapid and perhaps automatic identification and classification of such terrain features and characteristics. However, in all such applications, problems arising from a lack of homogeneity and isotropy of these features begin to play a stronger and stronger role as the sensing platform becomes more remote from the target scene, as in the airborne case, and especially when this concept is applied on a global basis from spacecraft platforms. Further, a degradation in the diagnostic potential of unique spectral patterns may be expected to result from absorption, emission, and scattering effects in the intervening atmosphere. At present, the prediction of such effects,which can be expected to vary considerably with variations in atmospheric conditions,is uncertain. As a direct result it is not presently possible to correct data taken at altitude for such effects.

These two problems, homogeneity and atmosphere, present somewhat different experimental ground rules on equipment performance requirements. For example, the operational generation of spectra for identification of terrain features requires a spatial resolution compatible with their size, homogeneity, and isotropy. For features of interest to most users this

may be a considerably more rigid requirement than the spatial resolution necessary for a study of atmospheric effects. The latter may be satisfactorily accomplished with relatively relaxed spatial resolution requirements through measurement over ocean areas or extensive, uniform land features such as snow-covered terrain.

A final decision regarding optimum spatial resolution must therefore be the result of studying several interrelated factors arising from equipment considerations, vehicle capabilities, and mission goals. Considering first the resolution requirements established by the user's goals concerning detection and identification, it appears that ground-resolution cell sizes in the range of 4 to 100 ft are usually specified [1] at least in the preliminary, multidiscipline approach to orbital experimentation. As future special purpose instruments become necessary, more closely defined resolution requirements will probably arise. The determination of a desirable ground-resolution cell size must also include a consideration of several other parameters such as platform altitude and forward velocity (and hence ground smear), maximum tolerable data rate, and data storage or transmission capabilities. However, a sizeable amount of very useful information can be obtained from spectrometer data representing a considerably larger ground-resolution cell size (for example, atmospheric effects over an extensive, uniform terrain feature), and an initial model spectrometer need not necessarily realize high spatial resolution.

Nevertheless, in order to evaluate system performance it is instructive to consider a system design capable of spatial resolution compatible with terrain features of interest to the various user agencies, perhaps for example, a ground-resolution cell of 50 ft. These results can then be scaled to any other less stringent resolution requirement according to the performance equation presented in the previous section. Consider first the effect of platform altitude. Equipment capabilities are presently compatible with a ground-resolution cell size of 50 ft from aircraft (but probably not from spacecraft) altitudes. For example, from anticipated aircraft altitudes (to perhaps a maximum of 40,000 ft) a 1 mrad spatial resolution would be acceptable, giving an instantaneous resolution cell size of no more than 40 ft at the ground.

The next consideration involves allowable ground smear and/or image motion compensation (IMC) which are both intimately linked with the maximum tolerable data rate. Again recalling the airborne case, it is certainly possible to encounter velocity to height (v/h) ratios varying from 0.02 to 0.2 rad/sec (e.g., a 40,000-ft aircraft flying at 800 fps or a 1000-ft flight at 200 fps). Thus, even if we were to accept a one-resolution-element ground smear during a given spectral scan (1 mrad), we are faced either with the potential requirement for up to 200 complete spectral scans per second or the introduction of image motion compensation perhaps at the expense of contiguous coverage.

Contiguous sampling would not be necessary for some applications. However, boresighting with an imaging system is unlikely to remain perfect in practice so that assignment of the

recorded spectra to specific objects on the ground track will be greatly facilitated if contiguous sampling can be used.

While the requirement for 200 spectral scans per second (over an as yet undefined spectral range and at an unspecified spectral resolution) may well create an unacceptable data rate, an equally important consideration arises from the fact that ground smear may negate the potential benefit of multispectral data gathering, since data obtained in different spectral intervals will correspond to physically different elements of the scene.

In general, as the platform altitude is increased v/h will decrease, thereby reducing the system's electrical bandwidth requirements (data rate) for achieving contiguous or near-contiguous coverage. However, a simultaneous increase in ground-resolution cell size (for constant system angular resolution) together with known homogeneity and isotropy of terrain features will severely limit the acceptable ground smear for some applications. Thus, with an angular resolution which appears reasonable for future operational data collection (limited by system sensitivity), it seems that some form of image motion compensation will be required as altitudes are increased toward orbital values, regardless of system bandwidth capabilities.

Since one important function of an airborne spectrometer will be to develop and test techniques for use in an eventual spacecraft design, it seems highly desirable to include image motion compensation to assure spatial coincidence of better than 1/3 a resolution element throughout a spectral scan. Ultimately, as altitude (and therefore instantaneous resolution cell size) is increased and as systems become truly operational and less investigative in nature, the requirement for spatial coincidence may be expected to increase to 1/10 a resolution element or better.

The relative merits of automatic integration resulting from a ground smear of perhaps several resolution elements during a single spectral scan compared to high quality image motion compensation to achieve spatial coincidence throughout the scan, perhaps at the expense of complete ground coverage, will depend on the application. However it should be noted that this problem is alleviated if the required data rates for contiguous coverage (with image motion compensation) do not exceed sensor capabilities; i.e., it may be possible to achieve both spatial coincidence and contiguous coverage.

4.1.2.2. Diameter of the Collecting Optics. The minimum diameter of the collecting optics is a function of the system sensitivity required to achieve a desired SNR for a given change in scene reflectance. As such, it must be evaluated as a trade off between the required noise-equivalent reflectance difference (NE$\Delta\rho$), data rate capabilities (dwell time on each spectral and spatial resolution element), and overall size limitations.

A reasonable wavelength interval for an experimental short wavelength spectrometer is the 3-octave band, 0.35 to 2.8 μm, and a first consideration is the number of independent optical channels required to cover these three octaves of interest. There are numerous alter-

natives involving such factors as physical size and complexity, spectral scan rate, band coverage, and instantaneous spectral resolution. For example, one solution consists of an arrangement of several separate narrow-band filters spaced around the periphery of a wheel and sequentially rotated into the optical path. One advantage of such a system is the positive positioning and spectral band delineation which is possible. However, a disadvantage arises from the large number of individual filters (and consequently large size) required to achieve high spectral resolution over a reasonable spectral interval. It can be shown (see appendix) that in order to cover completely a spectral interval of N octaves at an instantaneous spectral resolution R (where $R = \lambda/\Delta\lambda$) a minimum of

$$n = R \ln 2N \tag{2}$$

individual filters is required, presuming optimum center frequency and bandpass characteristics. Thus, complete coverage of the 3-octave band of interest here (0.35 to 2.8 μm) with a spectral resolving power of say 33 ($\Delta\lambda/\lambda = 0.03$) would require at least 69 separate filters.

Ultimately, for high spectral resolution over a relatively wide interval it appears advantageous to use a continuously varying filter wedge. Such wedges can be fabricated with either linear or circular variation: the latter is recommended because it offers an obvious advantage in applications requiring cyclic spectral scanning at high scan rates.

Since a circular variable filter (CVF) commonly covers one octave, a maximum of three individual telescopes would be most efficient in terms of duty cycle: hence data rate per channel and ground smear (or IMC required) per scan are reduced. However, because the SNR increases by D^2 but only by $1/\sqrt{\Delta f}$, it is clearly advantageous to utilize any added size and weight in increasing the diameter of fewer, time-shared telescopes, subject to limitations established by increased data rates and possible reduction in sensitivity due to detector performance over multiple octave bands.

As a realistic compromise for a first iteration calculation, a single telescope with a 6 in. in diameter collector will be chosen. It remains to be determined if sequential scanning of the 3-octave band can be accomplished with an acceptable data rate and sufficient detector sensitivity throughout the spectral interval. Any difficulties in either area can quite likely be alleviated by either beam splitting or dual-channel optics.

4.1.2.3. Optical Path Transmission. The total optical path transmission is the straightforward summation of effects due to the atmosphere, collecting and focusing optics, and spectral filtering. Since no tradeoff relationships are involved, the only comment in this connection is that circular variable filter transmission will probably be as low as 15-20% in places. Except in the 1.38- and 1.88-μm water vapor bands, this will almost certainly be the most inefficient element in the optical path.

4.1.2.4. NE$\Delta\rho$. The overall system sensitivity, in terms of detectable reflectance changes in the scene, can be traded with any of the other design parameters governing achievable signal to noise. However, this parameter will ultimately be established by mission goals and by the magnitude of associated reflectance changes necessary for meaningful experimental conclusions. Since a primary goal of an airborne spectrometer program is a better definition of the requirements for diagnostic measurements, it seems reasonable to establish an NE$\Delta\rho$ of no more than 0.005 throughout the 3-octave band of interest. Better performance is theoretically possible over much of the wavelength range. However, target variability and the problems of handling wide dynamic range signals make it unlikely that greater accuracy would be worthwhile.

4.1.2.5. Spectral Detectivity of the Detector. The sensitive element is quite obviously limited by the operational wavelength band to such materials as PbS or InAs and possibly an S-20 photomultiplier for wavelengths below about 0.8 μm. Once again sensitivity may be traded for design complexity in terms of beam splitting, dual channel optics, detector cooling, cold shielding, etc.

4.1.2.6. Spectral Resolution. This parameter, like NE$\Delta\rho$, can be traded for other design criteria and will ultimately be established by mission goals and the information requirements to achieve these goals. As mentioned above, a primary goal of an airborne spectrometer measurement program is a more precise definition of the spectral resolution requirements for detection and identification of terrain features of interest to the user agencies. These features vary widely from the extent of snow cover in a particular mountain range to the classification of farm crops and ultimately to their state of vigor and projected productivity. Obviously such diverse mission goals will require equally variable resolution capabilities. However, in order to conduct an investigation of atmospheric effects on spectra to be obtained from these various missions, it is desirable to achieve the highest practical spectral resolution compatible with filter and system SNR capabilities. At present this is on the order of 0.03 λ across the 3-octave band of interest here (0.35 to 2.8 μm).

4.1.2.7. System Electrical Bandwidth. The most direct effect of spectral resolution trade off is in the required data rate capability. The minimum data rate required to cover a spectral interval of N octaves at an instantaneous spectral resolution $R = \lambda/\Delta\lambda$ can be shown to be (see app.)

$$\Delta f = \frac{v/h}{2\beta} R \ln 2N \tag{3}$$

Considering the most rigid requirements in terms of v/h (see sec. 4.1.2.1), a spatial resolution of 1 mrad and a spectral resolving power of 33.3, the need for a maximum electronic bandwidth of 6900 Hz is apparent. For the simplest optical system, a single-channel

CVF disc scanning the three octaves in succession, a detector time constant on the order of 50 μsec would be required.

A vast number of interrelated trade offs now arises. For example, at the other extreme of v/h (0.02), a spectral resolving power R = 20, and a higher duty cycle (three telescopes, each scanning one octave continuously), the allowable time constant is increased to over 1 msec. Detector time constant may be a limiting parameter in terms of sensor capabilities, and thereby establish limits for other system parameters.

4.1.3. SNR CALCULATION FOR TYPICAL SYSTEM. As discussed in section 4.1.2.1 through 4.1.2.7, various interrelated trade-offs and sensor capabilities indicate tentative system specifications for a 0.35- to 2.8-μm CVF spectrometer. In practice, this total wavelength interval should probably be reduced somewhat (to perhaps 0.4-2.5 μm) to allow for some overlap between commercially available 1-octave CVF filter segments. Typical values as discussed in the preceding sections may be used in equations 1 and 3 to yield the SNR performance for a reflective change $\Delta\rho$ of 0.005, or, alternatively, an NE$\Delta\rho$ for a SNR = 1.0 as shown in figures 1-3. In each case, three alternate systems are presented which represent different data rate capabilities. It should be noted that an allowable data rate establishes a specific physical configuration only for a given criterion of ground coverage. For example,

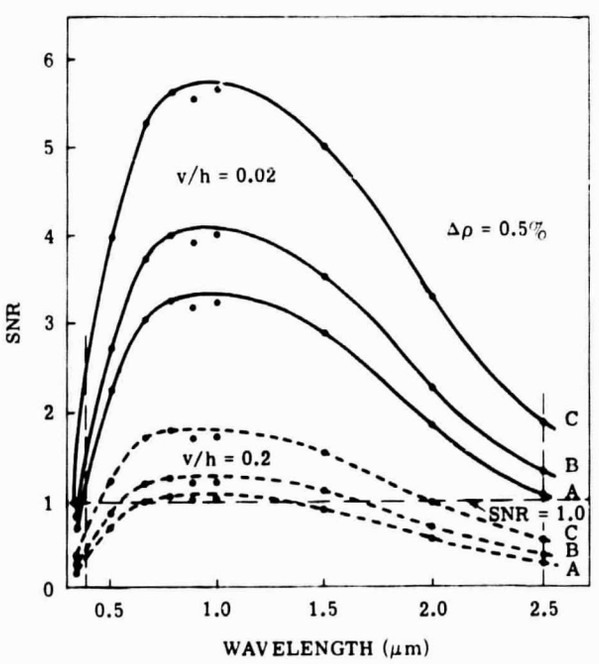

FIGURE 1. SNR PERFORMANCE FOR TYPICAL SYSTEMS

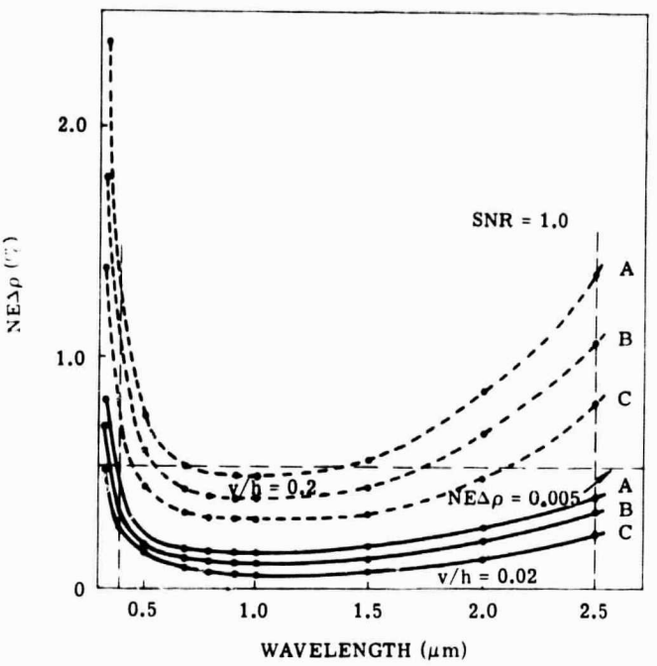

FIGURE 2. NEΔρ PERFORMANCE FOR TYPICAL SYSTEMS

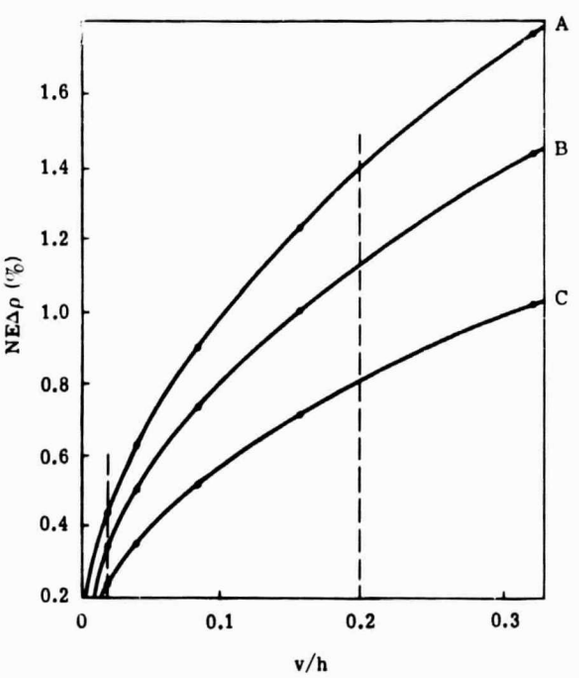

FIGURE 3. NEΔρ PERFORMANCE VS. v/h FOR SNR = 1.0

contiguous coverage with image motion compensation (or a ground smear of one resolution element without IMC) requires an electronic bandwidth Δf as given in equation 3. Thus for this case, one can consider the systems defined in table I. System A can realize performance identical to that shown for system C but only at the expense of a ground smear three times larger or alternatively one-third the coverage, given sufficient IMC. That is, trade offs are again possible among such factors as ground coverage, IMC, ground smear, SNR, and NE$\Delta\rho$ for any selected number of channels.

TABLE I. SYSTEM PERFORMANCE

	System A	System B	System C
	Single Channel (3 octaves on a single CVF disc)	Dual Channel (2 octaves on one CVF disc, 1 octave on second CVF disc)	Tri Channel (3 separate, one octave CVF discs)
	Δf(Hz)	Δf(Hz)	Δf(Hz)
v/h = 0.02	690	460	230
v/h = 0.2	6900	4600	2300

The performance of these three systems has been investigated using the following system specifications:

σ = 0.45

β = 1 mrad

D = 15 cm (f/2.0 optics required by CVF)

$\tau = (0.92)^4(0.175) = 0.125$ (ignoring atmospheric absorption)

$\Delta\rho$ = 0.005

R = 33.3

v/h = 0.02 to 0.2

Detector = uncooled PbS

$A_d = 0.02^2\ cm^2$

The results are illustrated in figures 1-3. It will be seen that the performance requirements are not met for the higher values of v/h. However, if an airborne instrument was needed to operate with highest sensitivity at high v/h, this could be achieved by means of a more complex system using an appropriate photomultiplier for the shortest waveband and a cooled detector (PbS or InAs) for the longest waveband.

4.2. ULTRAVIOLET IMAGING SYSTEMS: SCANNERS AND CAMERAS

The quantity of information collected by an imaging system is limited by three basic factors: dynamic range, SNR, and data rate. In making decisions concerning the type of imaging system to be employed in gathering pictorial data, each of these factors must be weighed along with the basic considerations of size, weight, cost, and data format.

Dynamic range is important because it determines the amount of information which can be obtained for each element of the scene. Anything which uses up dynamic range limits the utility of the system. One such limitation is dc bias (or fog) which occupies the lower levels and thus limits the range of the amplitude spectrum. A scanning device, because of its very nature, can easily accommodate for this through ac coupling. In obtaining imagery of small variations superimposed upon a large dc bias, the scanner can ignore the bias and thereby reserve its entire dynamic range for recording the more important variations in the scene.

A camera, on the other hand, is not so easily fashioned to meet the demands of such an application. The threshold speed, the exposure, and/or the contrast (γ) of the film can be adjusted through careful selection of emulsions, shutter speed, and/or development time or process in such a way that the dc bias does not expose the film. Within limits, this procedure can be used to ac couple the camera as well as the scanner, but with increased complexity and cost.

Signal-to-noise considerations are also of great importance, especially since the SNR determines how many levels can be distinguished within a given dynamic range. In a shot-noise-limited scanner, the noise increases proportional to the square root of the intensity of the radiation falling upon its surface. Thus, dc bias carried along with the signal (such as would be produced by scattering or haze in the ultraviolet spectrum) causes an increase in the noise which proportionately decreases the number of distinguishable levels within the dynamic range of the system.

With the camera system, the noise level is set by the granularity of the film. As shown in the following sections, the effect of high levels of haze is to force one to reduce directly the dynamic range of the usable portion of the information which does not lower the SNR but has the same effect as such a reduction would have because of the loss of dynamic range.

Assessments of data-rate and consequently of useful resolution are difficult to make because platform motion and present technology are limitations on the rate at which data can be obtained. It is certainly true that in the absence of platform motion the camera can collect useful data at a rate of billions of bits per second; no scanner has such a capability. Yet, for a given application, it is conceivable that the high data rate of the camera system will not be utilized; for example, if only one photograph is taken per second, a mean data rate equivalent to that of existing scanning systems results.

In the sections which follow, an effort is made to lay a groundwork for performing detailed studies of these topics. It should be noted that it is difficult to draw general conclusions. In theory, the ultimate limit will be set by the signal and noise of the sample of the radiation stream collected by the imaging system. This, in turn, depends upon the aperture and dwell time and is not dependent on the particular mechanism used to record the data. Practical aspects of the mechanism, as discussed above, will usually be the dominant factors, thus

making the comparisons discussed here necessary. It must be emphasized, however, that this study is only a beginning. Further research including detailed analyses of actual emulsions and other detection mechanisms will be necessary. The present study brings to mind a number of simple experiments which could be investigated. Both detailed analyses and simple experiments should be the subject of subsequent efforts in this area.

4.2.1. GROUND RULES. The purpose of this study is to consider the performance of cameras and scanners in the presence of atmospheric scattering or haze. For convenience, we compare the performance of two systems which are essentially comparable in the absence of haze, and we assume that haze produces a dc bias that can be eliminated in the scanner through ac coupling (with dc-level monitoring if absolute levels are of interest). The question is then whether the camera can be modified to make the haze of no consequence without loss in sensitivity or dynamic range in excess of that evidenced in a shot-noise-limited (photomultiplier) scanner.

4.2.2. ANALYSIS. The total brightness (B) observed at a given camera station can be considered as the sum of the transmitted scene brightness (τB_s) and the atmospheric path radiance (B_a)

$$B = B_a + \tau B_s \tag{4}$$

where B = measured brightness
B_a = atmospheric brightness
B_s = scene brightness
τ = atmospheric transmittance

Studies of atmospheric illumination levels related to the early Gemini flights indicate that in the region from 0.35 to 0.5 μm it is not unusual for the atmospheric brightness to greatly exceed the transmitted brightness. As a result the apparent scene modulation is greatly reduced, giving the appearance of reduced resolution and producing a low-contrast image. The actual scene modulation M_o is defined by

$$M_o = \frac{B_h - B_l}{B_h + B_l} \tag{5}$$

where the subscripts h and l refer to the scene highlight and lowlight brightnesses. In the presence of haze, the apparent modulation M at the camera station is calculated by combining equations 4 and 5 to obtain

$$M = \frac{\tau(B_h - B_l)}{\tau(B_h + B_l) + 2B_a} \tag{6}$$

The ratio of transmitted to original scene modulation, called the modulation transmittance, is given by

$$\frac{M}{M_o} = \frac{1}{1 + \frac{2B_a}{\tau(B_h + B_l)}} \tag{7}$$

Using data from reference 2, values of M/M_o for typical average scene brightness levels (from 40 to 160 ft-L), viewed at satellite altitudes, range from 0.105 to 0.060 corrected for the human eye (which has a peak response at 0.55 μm). Assuming a modest increase in B_a/τ due to increased scattering at shorter wavelengths, it is clear that the atmospheric brightness at about 0.4 μm will exceed the average transmitted scene brightness by factors of about 20 to 80.

So far, we have not discussed how these factors affect scanners and cameras. It is evident that the reduction in apparent scene brightness and the reduction in scene modulation are atmospheric effects and will affect both sensors equally. As shown in reference 3, the SNR of a shot-noise-limited scanner is

$$\Delta(\mathrm{SNR}) = K\,\Delta B_s \sqrt{\frac{1}{B_a + \tau\bar{B}_s}} \tag{8}$$

where K = constant related to system parameters

ΔB_s = change in scene brightness

B_a = atmospheric brightness

$\tau\bar{B}_s$ = average apparent scene brightness

It is evident, then, that the effect of the haze levels discussed previously will be to reduce the SNR by a factor of four to nine from the no-haze condition. Assuming a constant dynamic range, this means that the total number of distinguishable brightness levels will be reduced by a factor of four to nine times, which is a considerable loss.

Analysis of the photographic situation is not nearly so straightforward. Of necessity, this part of the analysis is longer and more involved than for the scanner and yet less conclusive. It is in this area that further study is deemed necessary.

Since the end product of the photographic system is the photograph, it is instructive to confine our discussion to emulsion-related effects. On the finished negative, the density variations will be related to the scene brightness in a relatively straightforward fashion. In terms of density, the image modulation (M') will be given by

$$M' = \frac{D_h - D_l}{D_h + D_l} \tag{9}$$

where D = density of photographic image at the point of interest. If the situation encountered is normal low-haze photography, maximum information storage is obtained by adjusting the shutter speed and development time or process until D_l corresponds to the fog level and until D_h corresponds to film saturation of the film, as shown in figure 4.

As shown in figure 5, the introduction of haze has two primary effects: reduction of apparent scene brightness range through atmospheric attenuation and increase of apparent

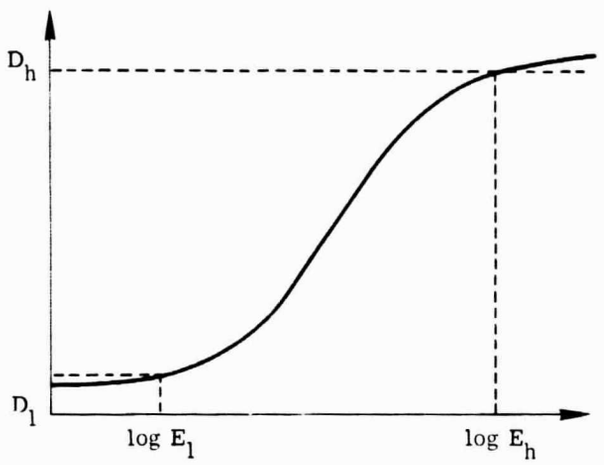

FIGURE 4. CHARACTERISTIC CURVE FOR AN EMULSION

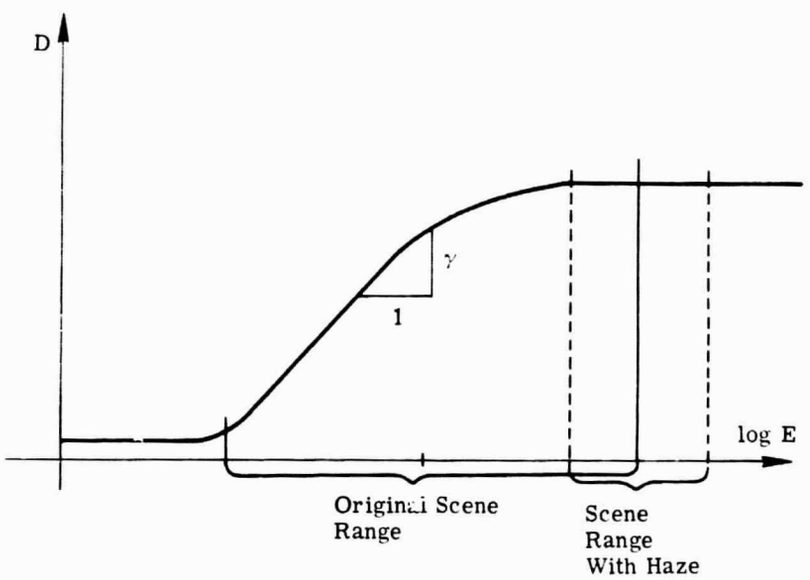

FIGURE 5. EFFECTS OF INTRODUCING HAZE

brightness level through scattered light. Since the D-log E curve for the original scene does not match the situation with haze (because of poor utilization of the exposure latitude and consequent wasting of usable dynamic range), the low-light exposure and film gamma should be altered as shown in figure 6. The question is now whether film characteristics can be so easily altered that this simple solution is practical.

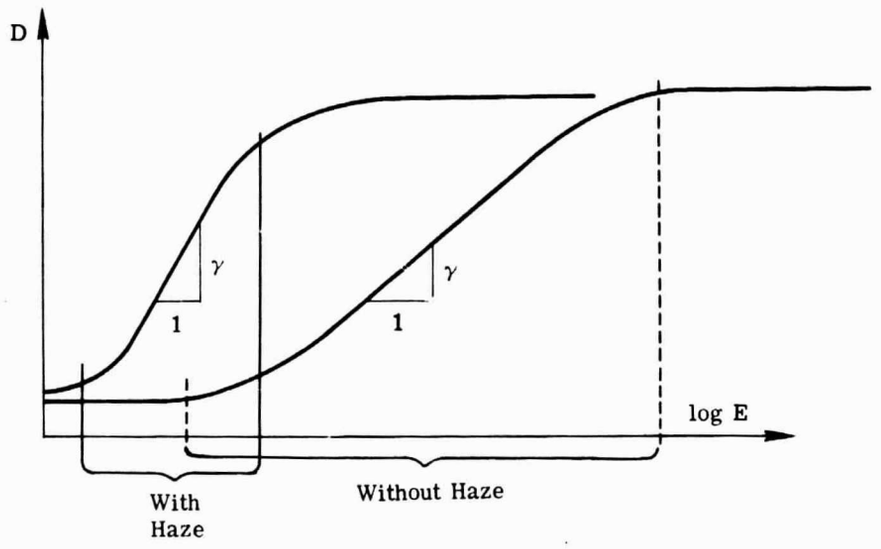

FIGURE 6. FILM MODIFICATIONS FOR ONE SCENE WITH AND WITHOUT HAZE

The information capacity of a photographic emulsion is limited by the fluctuations in density which occur even if the emulsion is exposed uniformly. It has been shown that, for a given mean density level, the product of the rms sensity fluctuation σ and the square root of the area of the scanning aperture A or the measuring instrument is invariant [4]: i.e., the Selwyn granularity is constant. It has also been shown that, for film resolutions from 10 to 100 lines/mm, the granularity tends to increase as the square root of the mean density level. Analytically, then, σ is described by

$$\sigma = kA^{-1/2}D^{1/2} \tag{10}$$

where k is a constant for the emulsion related to the effective cross-sectional area a of the grains as follows [5]

$$k = 0.66a^{1/2} \tag{11}$$

Thus, the rms density fluctuation is

$$\sigma(D) = 0.66(a/A)^{1/2}D^{1/2} \tag{12}$$

Assuming that the fluctuations have a Gaussian probability distribution, there is a 68% probability that a given exposure E_i will give rise to a density value in the range $D_i \pm \sigma_i$, a 95% chance that it will fall in the range $D_i \pm 2\sigma_i$, etc.

It is seen, then, that a quantization of density levels has been forced upon the otherwise continuous characteristic curve of an emulsion. Customarily, a distinguishable density level (DDL) is taken to be all densities within the range $D_i \pm \sigma_i$, even though this leads to overly optimistic results in terms of reliability [6].* Accepting this definition of a DDL, there exists a limited number N of such levels within the usable density range (which we will define as $D_l < D < D_h$) of a given emulsion. The value of N may be computed as follows: consider an infinitesimal density change dD. Since a change equal to 2σ will result in a change of N = 1, the infinitesimal change results in a $dN = dD/2\sigma$. Integrating, we obtain

$$N = \int_{D_l}^{D_h} dD/2\sigma$$

or using equation 12

$$N = \frac{1}{1.32(a/A)^{1/2}} \int_{D_l}^{D_h} D^{-1/2} dD$$

or

$$N = \frac{D_h^{1/2} - D_l^{1/2}}{0.66(a/A)^{1/2}} \tag{13}$$

In order to use this result, it is first necessary to obtain realistic values for a, the effective cross-sectional area of the grains in the emulsion. The values for the effective grain diameters for typical films are tabulated in table II (derived from reference 4).

TABLE II. EFFECTIVE GRAIN DIAMETERS FOR TYPICAL EMULSIONS

Film Type	Effective Grain Diameter (μm)
Royal X Pan	5.20
Panatomic	2.25
Plus-X Negative	2.15
Fine Grain Release Positive	0.95

* This situation is comparable to the choice of SNR = 1 for defining reflectance-difference sensitivities of scanning devices. In either case, the reliability is about 68%.

Generally speaking, for most films the density latitude yields a value for $D_h^{1/2} - D_l^{1/2}$ equal to about 1.3, so that N can be written as approximately $2\sqrt{A/a}$. The number of DDL's for the emulsions of table II will be approximately those listed in table III.

TABLE III. DISTINGUISHABLE DENSITY LEVELS FOR TYPICAL EMULSIONS

Film Type	Resolution (line/mm)		
	10	20	50
Royal-X Pan	38	19	8
Panatomic-X	89	44	18
Plus-X Negative	93	46	19
Fine Grain Release Positive	212	106	42

With regard to the granularity effects, it can be seen that haze is especially deleterious since it tends to occupy the lower range of densities where most of the DDL's are concentrated. This may be illustrated as follows: consider an emulsion for which $D_l = 0.36$, $D_h = 3.60$, and $\gamma = 1.0$. Half of the DDL's will be located in the range from D_l to $\left(\frac{D_h^{1/2} + D_l^{1/2}}{2}\right)^2$, or from D = 0.36 to D = 1.56. Since $\gamma = 1$, this corresponds to a range of log E equal to 1.2 (out of a total range of 3.24), which in turn corresponds to 1% of the total exposure range. It is exactly this kind of sensitivity to haze which complicates the ac coupling of the photographic imager.

Where the dc bias introduced by haze is very small compared with the apparent scene modulation, it becomes relatively simple to diminish its effects by reducing the exposure time until the haze exposure is less than the fog level of the film. A brief consideration of the characteristic D-log E curve of a typical emulsion will lead to conclusions of what must be done as the haze component increases relative to the scene.

In the linear portion of the D-log E curve, the density varies with exposure according to the relation [see fig. 7].

$$D = \gamma \log (E/E_o)$$

For a given photograph, the range of densities from lowlight to highlight conditions is

$$D_l \leq D \leq D_h$$

where $D_l = \log [(E_l + E_a)/E_o]$

$D_h = \log [(E_h + E_a)/E_o]$

E_a = atmospheric illumination exposure (haze)

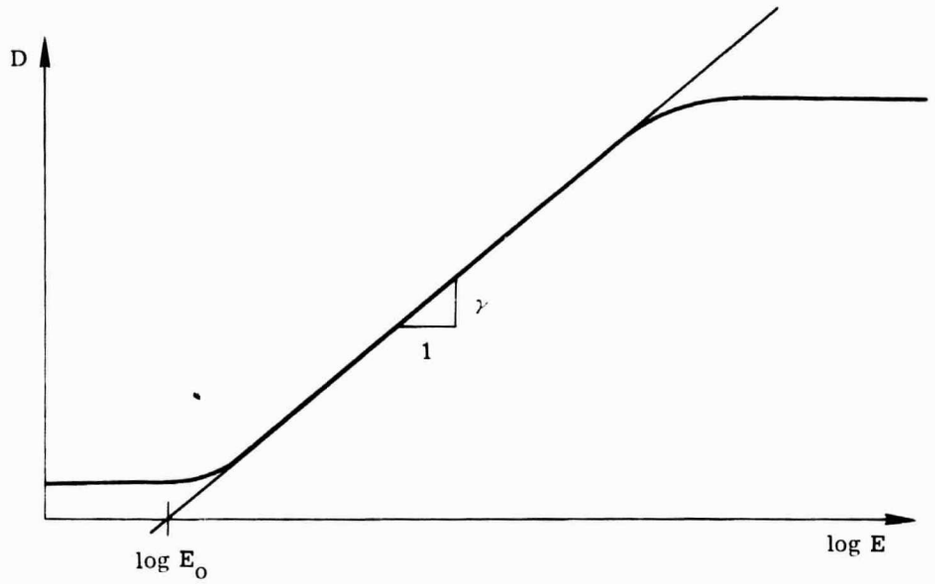

FIGURE 7. CHARACTERISTIC CURVE FOR A TYPICAL PHOTOGRAPHIC EMULSION

Thus, the total range of densities displayed is

$$D_h - D_l = \gamma \log |(E_h + E_a)/E_o| - \gamma \log |(E_l + E_a)/E_o|$$

or

$$D_h - D_l = \gamma \log |(E_h + E_a)/(E_l + E_a)| \tag{14}$$

Typical photographic emulsions have a density latitude (within the linear portion of the characteristic curve) of approximately 2. Thus, the necessary γ to accommodate the scene modulation can be determined by using $D_h - D_l = 2$ in the following form of equation 14

$$\gamma = 2/\log |(E_h + E_a)/(E_l + E_a)|$$

If E_l is chosen to be zero, i.e., if targets of zero reflectance are taken as a reasonable minimum, then we may write for the required γ

$$\gamma = 2/\log (1 + E_h/E_a) \tag{15}$$

A graph of this function is shown in figure 8. For a density range of 2, only about 25% haze can be accommodated by ordinary films ($\gamma < 3$).

For greater haze levels, it becomes necessary to use the maximum γ (e.g., $\gamma = 3$) but to accept some reduction in $D_h - D_l$, with a consequent reduction in the number of information-carrying DDL's. With $E_a >> E_h$, equation 14 becomes (using a simple MacLaurin's series)

$$D_h - D_l = 0.43\gamma(E_h/E_a) \tag{16}$$

Since the maximum practical value for γ is about 2.8, this says that $D_h - D_l \cong 1.2(E_h/E_a)$ is a practical maximum for high-haze conditions.

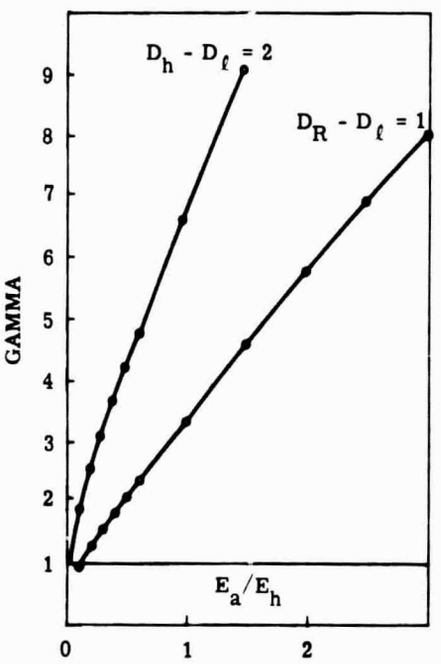

FIGURE 8. FILM CONTRAST VS. RATIO OF ATMOSPHERIC HAZE TO SCENE HIGHLIGHT ILLUMINATION

One relevant observation is that it is conceivable that the total useful density range in high-haze photography might represent less than one DDL. For example, with Plus-X aerial negative film, the practical high γ is 2.2, with a fog-level density of 0.12 [7]. Thus, with $E_a/E_h = 80$ (a practical value) the total information-carrying density range is 0.011; for such density levels, one DDL is $2\sigma = 1.32 \times (0.00215R)(0.125)^{1/2}$ or $2\sigma = R \times 10^{-3}$ where R is the number of lines per millimeter in the finished product. Setting 2σ equal to the total information-carrying density range of 0.011 yields R = 11 lines/mm which is a typical value for remote sensing scanner imagery. It must be noted, however, that only a 68% reliable on-off indication would be possible even at this low a resolution for a haze level equal to 80 times the nighlight illumination. Since the same emulsion can produce 90 DDL's at the same resolution in the absence of haze, the haze has degraded performance over 90 times. As mentioned earlier, the scanner's dynamic range is reduced by a factor of 9 under the same conditions. Although

other factors would have to be considered (e.g., initial film resolution, data rate, etc.) it is evident that the haze has a far greater effect on the camera than it does on the scanner imagery.

Consider an aerial ultraviolet-scanner display with a spatial resolution of 10 lines/mm and a dynamic range of 200 levels (i.e., $NE\Delta\rho = 0.005$). Consider also a camera system with fine grain release positive film capable of the same resolution and the same dynamic range (see table III). In the absence of haze, and with suitable associated hardware, the performance of these two systems would be identical. As shown earlier, the effect of atmospheric haze which is 80 times the apparent scene modulation is to degrade the scanner dynamic range to 22 levels and the camera's dynamic range to 2 levels. The conclusion is obvious in this case.

Matters are complicated further in high-gamma photography, since one consequence of increased γ is increased fogging of the film. As shown in figure 9, the fog-level density of typical aerial films increases as γ^n increases, where n may be anything from 1 to ∞ but is usually between 1 and 5. This means that any gain brought about through increased γ may be lost through the loss of valuable DDL's at low density levels, even though increasingly higher densities are obtainable as γ is increased. With Kodak Special Fine Grain Aerial Film, for example, an 8% loss in DDL's is experienced with a 50% increase in γ.

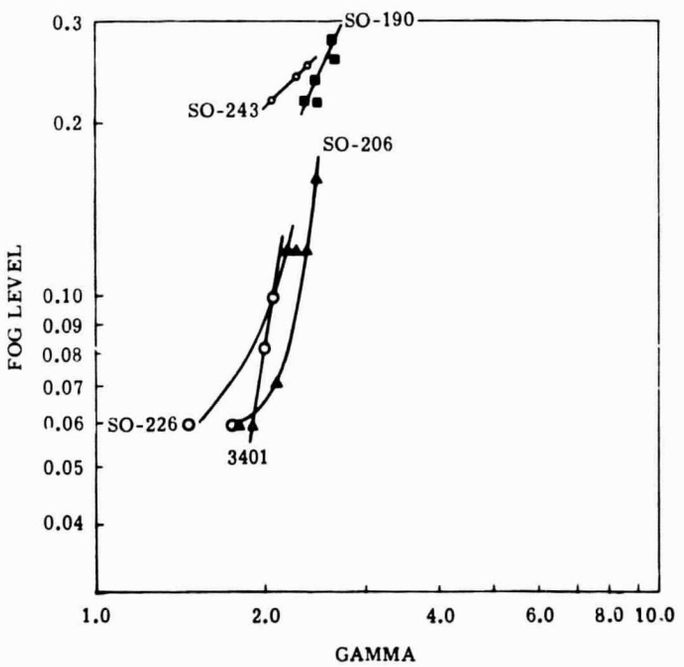

FIGURE 9. RELATIONSHIP OF FOG LEVEL TO FILM GAMMA.
Information is taken from data in reference 7.

4.2.3. CONCLUSIONS. It has been shown that using the ground-rules presented in section 4.2.1, an ultraviolet-sensitive camera can perform as well as a scanner in the presence of haze, provided that the dc bias introduced by the haze is less than 25% of the apparent scene modulation. As the haze increases in severity, the performance of the scanner tends to degrade more slowly than that of the camera. However, it must be understood that insufficient data and analysis have been presented to warrant any further conclusions at the present time.

4.3. EFFECTS OF PATH ABSORPTION

It has become increasingly appreciated in recent years that optimum utilization of remote sensing systems requires use of the information contained in the intensity and spectral character of the radiation sensed. In fact, for many applications, the spectral distribution of radiation intensity or spectral signature of the object viewed can afford identifications or discriminations which would be impossible based upon geometric shape alone. In view of this, it has become increasingly important to understand the effects of variable atmospheric path (i.e., varying altitudes) upon spectral signatures.

4.3.1. SPATIAL RESOLUTION EFFECTS. The spatial resolution of either photographic or optical-mechanical scanner imagery generally has the form of constant angular resolution so that the linear resolution at the ground is directly proportional to the altitude. This result can, of course, be altered by changing the focal length of the objective lens or mirror and by making other appropriate changes to the equipment. This involves a simple geometric relation which can readily be accounted for. It is more important to note that there are less obvious effects which may degrade resolution but which are likely to become less important as altitude is increased or to produce a constant degradation of the angular resolution. The degradation of ground resolution due to scintillation caused by atmospheric turbulence will, for a given atmospheric condition, become less noticeable as the altitude is increased since for constant angular resolution the geometric ground resolution will fall off with altitude. In any case, scintillation effects are likely to be relatively insignificant for most aircraft and satellite applications except, perhaps, for some specialized situations such as oblique photography using lenses with very long focal lengths. If aircraft-induced turbulence leads to significant scintillation, this would no longer be true. Such effects, however, are believed to occur only in certain regimes of high-speed flight with which most applications need not be concerned.

Aircraft vibration and instability may lead to image resolution degradation resulting from motion of components in the imaging system during exposure. Usually such vehicular motion is reduced in magnitude as altitude is increased, so that performance degradation by these parameters with increasing altitude is unlikely. Particular aircraft operating conditions which lead to excessive vibration or instability can usually be avoided.

It is often supposed that haze can lead to spatial resolution degradation. However, it has been shown by Middleton [8] and others that this is not the case except perhaps under very

special circumstances such as when a very thin layer of dense fog is almost in contact with the target. Middleton also demonstrates that the more general and more important effect of haze is to destroy the contrast in the image by the dual action of scattering radiation reflected or emitted by the target out of the beam and by scattering radiation from any other source into the beam.

4.3.2. PATH ABSORPTION AND SCATTERING EFFECTS. The effect of sensor altitude upon the apparent radiance of a target at the earth's surface which fills the sensor's instantaneous field of view can be ascribed to two simultaneous processes. The matter in the atmospheric path between the target viewed and the sensor (1) attenuates by absorption or scattering the radiation emanating (by reflection or self emission) from the target and (2) scatters and emits unwanted radiation into the field of view so that it appears to come from the target. These effects can be shown in equation form as follows: if $N^t\lambda$ is the actual spectral radiance of the target t in a small spectral bandwidth λ then the apparent radiance $N^t_{(\lambda,h)}$ sensed vertically from altitude h is given by

$$N^t_{(\lambda,h)} = \tau^P_{(\lambda,h)} N^t_\lambda + N^P_{(\lambda,h)} \tag{17}$$

where $\tau^P_{(\lambda,h)}$ is the path-transmission coefficient which indicates the degree to which the actual target radiance is attenuated, and $N^P_{(\lambda,h)}$ represents the extraneous radiation emitted or scattered by the atmosphere into the beam collected by the sensor. The path transmission coefficient and path radiance are functions of λ, h, and the atmospheric conditions.

It is interesting to delve into the implications of equation 17 in order to visualize at least qualitatively how such an altitude-radiance relationship affects the remote sensor data. In particular, one would like to know not only how the apparent radiance of a given target is modified but also how the radiance difference between two or more targets is affected.

In order to observe the effect of altitude upon a given target's apparent radiance, the relation of equation 17 may be differentiated relative to altitude h producing

$$\frac{\partial}{\partial h}\left(N^t_{(\lambda,h)}\right) = \left(N^t_\lambda\right)\frac{\partial}{\partial h}\left(\tau^P_{(\lambda,h)}\right) + \frac{\partial}{\partial h}\left(N^P_{(\lambda,h)}\right) \tag{18}$$

Now $\frac{\partial \tau^P}{\partial h}$ has a negative value since the overall transmission of the path decreases as path length increases. On the other hand, $\frac{\partial N^P}{\partial h}$ has a positive value since (except for some unusual circumstances) the amount of radiation scattered or emitted by the atmosphere into the sensor's field of view increases as the amount of particulate matter in the atmospheric path between sensor and target increases. Consequently, the direction of the net change in altitude of the apparent target radiance will depend upon the relative magnitudes of $\frac{\partial \tau^P}{\partial h}$ and $\frac{\partial N^P}{\partial h}$ and upon the magnitude of the actual target radiance. For instance, it can be seen that if the

actual target radiance N_λ^t were quite small, then the positive term $\frac{\partial N^P}{\partial h}$ in equation 18 could dominate so that the apparent target radiance $N_{(\lambda,h)}^t$ would increase with altitude. Conversely, if the actual target radiance were quite large, then the negative term $\left(N_\lambda^t\right)\frac{\partial \tau^P}{\partial h}$ could dominate, thus producing a decrease in apparent radiance with altitude.

The radiance difference between two targets, a and b, of actual radiance N_λ^a and N_λ^b, respectively, is given by

$$\Delta N_\lambda^{(a,b)} = N_\lambda^a - N_\lambda^b \tag{19}$$

The effect of altitude upon this difference can be seen by using equation 17 to obtain

$$\Delta N_{(\lambda,h)}^{(a,b)} = N_{(\lambda,h)}^a - N_{(\lambda,h)}^b = \left(\tau_{(\lambda,h)}^P N_\lambda^a + N_{(\lambda,h)}^P\right) - \left(\tau_{(\lambda,h)}^P N_\lambda^b + N_{(\lambda,h)}^P\right)$$

or, substituting equation 19

$$\Delta N_{(\lambda,h)}^{(a,b)} = \tau_{(\lambda,h)}^P \Delta N_\lambda^{(a,b)} \tag{20}$$

Equation 20 predicts that the apparent radiance difference between two targets is affected only by atmospheric transmission changes as altitude increases and is independent of the level of path radiance $N_{(\lambda,h)}^P$ since the latter quantity cancels in the differencing. As stated previously, the path transmission will decrease with increasing altitude. Consequently, equation 20 indicates that the apparent radiance difference between two targets will always decrease with increasing altitude.

4.3.3. APPLICATION OF THE ALTITUDE EQUATIONS. These equations could be used in two ways. If some areas of known radiance are mapped with the multispectral sensor, then the equations could be used to deduce the unknown values of path absorption and radiance. These could then be used to find true values of spectral radiance of other targets in the same locality for which the newly deduced absorption and radiance values can reasonably be expected to hold. Alternatively, radiance and absorption values deduced from meteorological data could be used to correct observed values.

When it is desirable to use true surface radiance, it is clear that, as far as possible, observational wavelengths should be used for which the path absorption and radiance are small. For example, to estimate surface temperatures from measured radiances, usually, the clear regions of the 10-μm atmospheric window are used. From orbital altitudes, the optimum region is from 10.5 to 12.5 μm, as wavelengths below 10.5 μm are unduly affected by the 9.6-μm ozone band and wavelengths longer than 12.5 μm are affected by the cluster of CO_2 bands centered on 15 μm. While this region is one of the clearest wavelength bands available, the residual absorption is sufficient to have appreciable effects on the observed radiance.

In the absence of cloud and scattering particles, the absorption within the 10.5- to 12.5-μm region is due primarily to the far wings of the intense water vapor lines at both shorter and longer wavelengths. The absorption coefficient is almost constant across this region, in contrast to the rapid and irregular variations which occur at most other wavelengths due to the complex line structure of the absorption bands. As a result, it is possible to carry out calculations of the absorption and emission effects in this window in a relatively straightforward way provided that the temperature and humidity profile of the atmosphere are known.

In order to illustrate these effects and obtain their orders of magnitude, calculations have been carried out for the U. S. Standard Atmosphere using data given in reference 9. For this atmosphere the surface air temperature is 15°C (59°F) and the lapse rate is 13° per 2-km height interval. There are 1.12 cm of precipitable water in the lowest 2-km layer, but the water content falls rapidly to 0.0022 cm between 10 and 12 km and there is only 0.0041 cm above 12 km. Using a value of 0.1 $cm^2\ gram^{-1}$ for absorption coefficient in the 10.5- to 12.5-μm band due to each gram of water in a column of 1-cm^2 cross section [9] the emittance of each 2-km layer was calculated together with the absorption of the path above each layer. Then by summing the contribution from each layer and the surface (which is assumed to have an emissivity of unity) the apparent radiance as viewed from above the atmosphere is obtained. The calculation is summarized in table IV.

We see that absorption in the vertical path reduces the emittance from the surface by an amount corresponding to a reduction in surface temperature of around 12°. However, when emission is also considered, the error for the example chosen is only about -3°. The relative humidity over the altitudes at which there is appreciable water vapor in the standard atmosphere used in the example varies between 60 and 77%. As the total path absorption is only 17% we can consider that the effects will be proportional to the humidity levels. Thus for 100% relative humidity the error would be increased from -3° to around $-4\ 1/2^{\circ}$, while for zero humidity the error would, of course, be zero. In fact it would appear that for temperate surface conditions even in the absence of detailed synchronous meteorological information, it would be possible to estimate the path humidity and temperature profiles from seasonal data well enough to predict the error to within about $\pm 1\ 1/2^{\circ}$. With weather charts it should be possible to reduce the error to about $\pm 1/2^{\circ}$.

It should be noticed that the apparent temperature differences between the three surface temperatures considered are 4 and $4\ 1/2^{\circ}$ compared with the actual differences which are 5°. Thus, the errors in temperature differences are less than those in the temperatures themselves. Using even crude meteorological data these small errors could be reduced to perhaps $1/2^{\circ}$.

The actual water content of the path is a steep function of temperature as well as of relative humidity. As a direct result, the absorption and emission effects will be reduced in cold weather toward the poles while they will be increased in hot weather toward the equator. This

TABLE IV. PATH ABSORPTION AND EMISSION EFFECTS AT 10.5 TO 12.5 μm FOR U. S. STANDARD ATMOSPHERE

Layer (km)	Mean Temperature T (°C)	Centimeters of H_2O in Layer	Centimeters of H_2O in Superior Column	Emittance of Layer ϵ	Transmission of Superior Column τ	$\epsilon\tau$	11.5 μm Blackbody Emittance M_T	Apparent Emittance $\epsilon\tau(M_{T-2})$ (W/cm-sr^{-1})
	20						26.3	21.8
Surface	15		1.94	1.0	0.83	0.83	24.6	20.4
	10						22.8	18.9
0-2	9	1.12	0.82	0.1	0.92	0.092	22.5	2.07
2-4	-4	0.52	0.30	0.05	0.97	0.049	18.0	0.88
4-6	-17	0.21	0.091	0.02	0.99	0.02	14.2	0.28
6-8	-30	0.07	0.021	0.007	~1.0	0.007	11.0	0.08
8-10	-43	0.015	0.006	0.0015	~1.0	0.0015	8.1	0.01
10-12	-53	0.002	0.004	--				

Path Emittance 3.32

Apparent Surface Temperatures as Seen from Above the Atmosphere at 11.5 μm

Surface Temperature (°C)	Path Transmission × Surface Emittance	Corresponding Temperature (°C)	Apparent Emittance from Above Atmosphere (i.e., 2 + 3.32)	Apparent Temperature (°C)
20	21.8	7	25.1	16.5
15	20.4	3	23.7	12.5
10	18.9	-1.5	22.2	8.0

effect is illustrated in table V in which the total path absorption has been estimated using several simplifying assumptions for a number of conditions.

By inspection of table V, it is clear that the errors will be much smaller and probably negligible for arctic conditions. On the other hand, for tropical conditions, the error will not only be about three times larger but about three times more uncertain due to the wider range of water vapor contents which can occur. It should also be noticed that changing angles of observation can affect the correction appreciably.

TABLE V. PATH TRANSMISSION

Vertical Path Transmission

Surface Air Temperature (°C)	100% Relative Humidity	66% Humidity	50% Humidity	30% Humidity
-40	0.998	0.999	0.999	- -
0	0.905	0.93	0.95	0.97
15	0.76	0.83	0.87	0.92
40	0.27	0.43	0.52	0.68
	40° Zenith Angle Path Transmission			
-40	0.997		0.998	
0	0.87		0.93	
15	0.70		0.83	
40	0.18		0.425	

Since the water vapor in the atmosphere is heavily concentrated at the lower levels, it is also clear that the elevation of the terrain may have a marked effect. From table IV it can be seen that over half of the water vapor is in the lowest 2-km layer. Thus, for a terrain elevation of 2 km (~6000 ft) the errors will be reduced to those calculated for zero elevation, all other things being equal.

The most important factor to be remembered, though, is the qualification that these arguments depend on the absence of particulate matter in the path. Opaque clouds make measurement of the surface impossible, but otherwise should present little problem unless perhaps they might be mistaken for snow cover. Low-altitude haze, though prevalent, occurs in continental regions and should present no problem since the absorption due to such haze is insignificant except for long horizontal paths close to the surface. Much more problematic are the thin and often invisible cirrus clouds whose presence has been indicated by results obtained in the TIROS and NIMBUS programs. These clouds are believed to have appreciable absorption and to be at altitudes producing well below surface temperatures. Thus, their emission will be insufficient to replace an appreciable fraction of the absorbed upwelling radiation. This problem is being studied by meteorologists. One feels that there should be

sufficient spectral information in the upwelling radiation to provide a solution to this problem: however, until such a solution is found the future of infrared measurements of surface temperatures must remain in doubt.

4.4. CRYOGENIC SYSTEMS

There are four basic techniques for cooling components such as infrared detectors for the remote sensing mission: liquid cryogens, solid cryogens, open- and closed-cycle refrigerators, and passive-radiation cooling. The characteristics of each mission (such as duration, operational duty cycle, equipment orientation, and accessibility for monitor and/or maintenance and temperature and heat load requirements) will determine which method is best suited to that specific application.

For example, ignoring strictly developmental situations, operational missions can be divided profitably into the airborne vs. spaceborne environment, since this primary distinction affects essentially all remaining characteristics for a given application. In an airborne situation, the duration is necessarily limited by other considerations to the extent that liquid cryogens offer the simplest and most reliable form of cooling. However, in a truly operational situation, this simplicity and reliability must be weighted against the cost and convenience features offered by modern mechanical refrigerators. Again, since mission duration and operational duty cycle are fairly well defined, equipment accessibility and relative ease of maintenance argue strongly for mechanical refrigerators. The primary trade offs between liquid cryogens and the refrigerator are overall cost, MTBF, and noise considerations due to temperature variations and/or mechanical vibrations. Weight and power requirements are normally of only secondary importance in the airborne situation.

The other two cooling techniques, solid cryogens and passive radiation, are, respectively, impractical and impossible on an airborne platform. Handling difficulties and cost alone make solid cryogens impractical for missions of duration certainly less than days and perhaps months.

In the spaceborne situation the case is not nearly so well defined nor, at this point, readily resolvable. Future decisions concerning the method to be selected will have to be made on the basis of the requirements such as flight duration and weight, size, power, and reliability considerations and on the current state of the art for each method. Here we merely list the advantages and disadvantages of the various alternatives as seen at the present time.

For intermittent operation with a long and indefinite hold time, the use of cryogenic gases stored under high pressure with open cycle (Joule-Thompson) cryostats appears attractive. However, the weight and explosion hazards of the storage cylinders make this method unattractive for extended observations or for manned earth resources missions, respectively. The use of open-cycle coolers with the working gas stored in the supercritical state was suggested for early manned flights of short duration. This was used in early manned flights since super-

critical gas storage has been highly developed and proved reliable in spacecraft life-support systems. However, for use under these circumstances it has probably been superceded by solid cryogens as discussed below.

Considering next the mechanical refrigerator, size and weight restrictions no longer appear very significant. Devices are presently available which weigh less than 10 lb and vary in their overall dimensions on the order of 3 in. × 10 in. to 4 in. × 12 in. Power requirements have also been reduced by more efficient design to the point that they are no longer intolerable. For example, commercial units are available with cold production of about 1/2 W at 77°K and 0.1 W at 35°K, requiring approximately 35-W input power. Certainly from the standpoint of operational convenience, this solution is superior to either solid or liquid cryogens and imposes no orbital or orientation constraints on the vehicle such as those associated with radiative cooling. The most severe limitations in the use of mechanical refrigerators arise from vibration, reliability, maintenance requirements, and operational duty cycle for extended missions. In general, commercially available units require maintenance at regular intervals measured in hundreds-of-hours operation. Recently available information indicates that at least for one unit, this may be extended to 3000-hr intervals with 10,000-hr MTBF (mean time before failure) which somewhat alleviates this problem. Vibration problems are also being solved by careful mechanical design. For missions of very long duration in situations allowing revisit at intervals of perhaps three months, the mechanical refrigerator may ultimately be the most practical solution to cryogenic requirements.

The use of solid cryogens for missions of long duration is also attractive because of their inherent simplicity, reliability, and relatively light weight. The solid cryogen system offers the advantages of passive operation, freedom from the venting problem associated with liquids in space, positive and predictable temperature control, freedom from undesirable vibration-induced noise, and long-lifetime continuous operation. Its major disadvantages are a relatively high cost and complex handling requirements in the prelaunch situation.

By varying the cryogen (or cryogen combinations in a dual design) operating temperatures can be varied down to about 8°K (solid hydrogen is at an equilibrium vapor pressure of about 0.1 torr). Total system weight and overall size are likely to be considerably larger than with miniature refrigeration for long lifetime operation. Nevertheless, it offers a very promising solution for flights of long duration (perhaps a year or so) with no revisit requirement.

Radiative cooling is an extremely desirable solution in terms of weight, reliability, temperature stability, cost, and operational simplicity. Its disadvantage is that constraints are imposed on the orbit and orientation of the spacecraft which could conflict with a given set of mission goals.

Thus, in summary, each mission presents specific operational demands and equipment limitations which must be evaluated in any decision concerning which mode of cooling is best suited to that mission.

4.5. OPTIMUM OPTICAL BANDWIDTHS FOR A MULTISPECTRAL SENSOR

Early in the development of multispectral sensors, it was realized that by dividing the radiation from an object into several spectral bands the number of distinguishable signatures could be greatly increased. This is illustrated by the example presented below which is followed by the proof of a general theorem on optimizing bandwidths and a brief discussion of the applicability of these ideas.

Suppose that a radiometer with a uniform spectral response from λ to $\lambda + \Delta\lambda$ but having zero response elsewhere is used to measure the reflectance of some target and that 100 different reflectances can be distinguished with this system. Then, if the spectral reflectivities in the bands λ to $\lambda + \frac{\Delta\lambda}{2}$ and $\lambda + \frac{\Delta\lambda}{2}$ to $\lambda + \Delta\lambda$ are independent, it would be possible using the same radiometer with different filters to distinguish 50 reflectances in each of these bands or $(50)^2 = 2500$ separate and distinguishable reflectance spectra. In fact, if we split $\Delta\lambda$ into n channels such that each has a dynamic range of 100/n the number of possible distinguishable spectra is $\left(\frac{100}{n}\right)^n$. We proceed to find the optimum value of n in the general case.

In general, if a dynamic range x is available in a given bandwidth, we can divide the distinguishable levels equally between n narrower bands. The number of distinguishable spectra is then

$$y = \left(\frac{x}{n}\right)^n$$

For convenience, we rewrite this in the form

$$\log y = -n \log n/x$$

and differentiating

$$\frac{1}{y}\left(\frac{dy}{dn}\right) = -\log n/x - 1$$

To find the maximum value of y we put $dy/dn = 0$. That is

$$\log x/n - 1 = 0$$

or

$$\log x/n - \log e = 0$$

giving

$$n = \frac{x}{e}$$

Thus the optimum dynamic range of each individual channel is $\frac{x}{n}$ or e.

As we could have chosen any value for λ and $\Delta\lambda$, this result is general; provided the reflectances in the subdivided channels are independent, the number of distinguishable spectra

is maximized by choosing the channel bandwidths such that the dynamic range in each channel is e (in general, the bandwidths of the several channels will be different).

It will be realized that this argument depends on other assumptions such as that the optical efficiencies and recording bandwidths per channel are independent of the number of channels. It is interesting to note, however, that the same result is obtained for a radiation-noise-limited system for which $y = k(\sqrt{x/n})^n$, and that the same result would be obtained for emissivity measurements. The restrictions, particularly that of independence, make the literal application of this result of questionable value. However, it should encourage workers in the field of multispectral remote sensing to use large numbers of channels at the expense of channel dynamic range when the inherent structure of the target spectrum warrants this.

5
CONCLUSIONS AND RECOMMENDATIONS

The work described in this report is part of an effort which should be continued. A proposal detailing the specific efforts recommended for the ensuing year was forwarded to MSC on 17 May 1968. A list of the studies recommended follows to indicate the direction in which it is felt this effort should proceed:

(1) Infrared detector cooling trade off studies
(2) Advanced infrared scanner conceptual design studies
(3) Prespaceflight checkout criteria studies
(4) Dynamic range/AGC requirements for space sensors
(5) Short wavelength spectrometer studies including breadboarding of key components
(6) Engineering support for NASA to provide data to substantiate engineering validity of proposed infrared experiments
(7) Assistance for NASA in establishing requirements to upgrade and develop new infrared equipment

APPENDIX: CALCULATION OF THE NUMBER OF RESOLUTION CELLS REQUIRED

In order to establish limiting detector time constants and electronic bandwidth requirements, it is necessary to determine the number of individual resolution cells (n) of given instantaneous spectral resolving power ($R = \lambda/\Delta\lambda$) required to completely cover a spectral interval (N octaves).

First note that $\Delta n_i = 1$ when $\Delta\lambda_i = \lambda_i/R$ and that

$$\frac{\Delta n_i}{\Delta\lambda_i} = \frac{R}{\lambda_i}$$

and

$$\frac{dn}{d\lambda} = \frac{R}{\lambda}$$

or

$$n = R\int_{\lambda_1}^{\lambda_2}\frac{d\lambda}{\lambda}$$

$$= R\,\ell n\,\lambda\Big]_{\lambda_1}^{\lambda_2}$$

Now for N octaves $\lambda_2 = 2N\lambda_1$ or $n = R\,\ell n\,2N$.

From information theory, we know that it is necessary to pass this many resolution elements/spectral scan times one-half the number of scans/second as defined by $\frac{V/h}{\beta}$, the ratio of V/h to the instantaneous spatial resolution; or (see fig. 10)

$$\Delta f = \frac{V/h}{2\beta}(R\,\ell n\,2N)$$

$$\lambda_i = \lambda_1 + \frac{1}{2}\Delta\lambda_1 = \lambda_2 - \frac{1}{2}\Delta\lambda_2$$

$$\therefore \lambda_2 = \frac{\lambda_1\left(1+\frac{1}{2R}\right)}{\left(1-\frac{1}{2R}\right)}$$

$$\lambda_3 = \frac{\lambda_2\left(1+\frac{1}{2R}\right)}{\left(1-\frac{1}{2R}\right)} = \frac{\lambda_1\left(1+\frac{1}{2R}\right)^2}{\left(1-\frac{1}{2R}\right)^2}$$

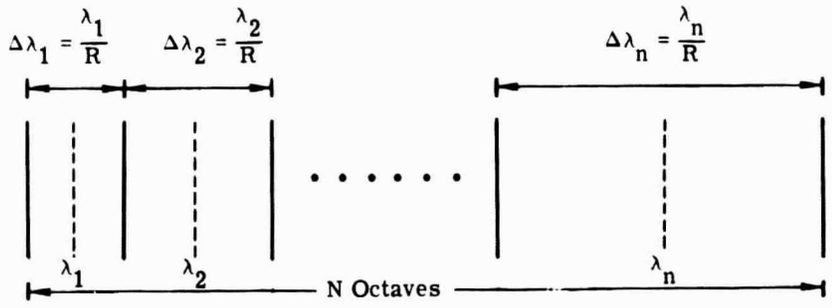

FIGURE 10. DISTRIBUTION OF RESOLUTION ELEMENTS

and

$$\lambda_n = \frac{\lambda_1\left(1 + \frac{1}{2R}\right)^{n-1}}{\left(1 - \frac{1}{2R}\right)^{n-1}}$$

but also

$$\left(\lambda_n + \frac{1}{2}\Delta\lambda_n\right) = 2N\left(\lambda_1 - \frac{1}{2}\Delta\lambda_1\right)$$

$$\lambda_n = 2N\lambda_1\frac{\left(1 - \frac{1}{2R}\right)}{\left(1 + \frac{1}{2R}\right)}$$

$$\therefore \frac{\left(1 + \frac{1}{2R}\right)^{n-1}}{\left(1 - \frac{1}{2R}\right)^{n-1}} = 2N\frac{\left(1 - \frac{1}{2R}\right)}{\left(1 + \frac{1}{2R}\right)}$$

$$n\,\ell n\left(\frac{1 + \frac{1}{2R}}{1 - \frac{1}{2R}}\right) = \ell n\ 2N$$

but

$$\ell n\left(\frac{1 + \frac{1}{2R}}{1 - \frac{1}{2R}}\right) = \left(\frac{1}{2R} - \frac{1}{4R^2}\right) - \left(-\frac{1}{2R} - \frac{1}{4R^2}\right) = \frac{1}{R}$$

$$= \left(\frac{1}{2R} - \frac{1}{8R^2} + \ldots\right) - \left(-\frac{1}{2R} - \frac{1}{8R^2} + \ldots\right) \neq \frac{1}{R} \text{ for large R.}$$

$$n\left(\frac{1}{R}\right) = \ell n\ 2N$$

$$n = R\ \ell n\ 2N$$

REFERENCES

1. I. Sattinger, Peaceful Uses of Earth-Observation Spacecraft, Vol. II, Report No. 7219-1-F(II), Willow Run Laboratories of the Institute of Science and Technology, The University of Michigan, Ann Arbor, February 1966.
2. A. R. Boileau, "Visibility," Appl. Opt., Vol. 3, May 1964, p. 549.
3. J. Braithwaite et al., An Investigative Study of a Spectrum Matching Imaging System, Report No. 8201-1-F, Willow Run Laboratories of the Institute of Science and Technology, The University of Michigan, Ann Arbor, October 1966.
4. G. C. Higgins and K. F. Stultz, "Experimental Study of rms Granularity as a Function of Scanning-Spot Size," J. Opt. Soc. Am., Vol. 49, No. 9, September 1959, p. 925.
5. J. A. Eyer, "A Limit on the Accuracy of Photographic Radiometry," Appl. Spectry, Vol. 14, No. 1, 1960, p. 4.
6. J. A. Eyer, "Influence of Emulsion Granularity on Quantitative Photographic Radiometry," Phot. Sci. Eng., Vol. 6, No. 2, 1962, p. 71.
7. H. J. Hall and H. K. Howell, Photographic Considerations for Aerospace, Itek Corporation, Lexington, Mass., 1966.
8. W. E. K. Middleton, Vision Through the Atmosphere, University of Toronto Press, 1958.
9. Shea L. Valley, Handbook of Geophysics and Space Environments, Air Force Cambridge Research Laboratories, L. G. Hanscom Field, Bedford, Mass., 1965.

DISTRIBUTION LIST

NASA Manned Spacecraft Center
Earth Resources Office
Houston, Texas 77058

ATTN: W. F. Eichelman/TE2 (25)
Contract NAS9-7156 (Plus 1 repro.)

NASA Manned Spacecraft Center
General Research Procurement Branch
Houston, Texas 77058

ATTN: R. L. Duppstadt/BG741
Contract NAS9-7156 (1)

NASA Manned Spacecraft Center
Technical Information Dissemination Branch
Houston, Texas 77058

ATTN: Retha Shirkey/BM6 (4)